Chinese Journal of Aeronautics, (2013),26(6): 1415–1421

Chinese Society of Aeronautics and Astronautics
& Beihang University

Chinese Journal of Aeronautics

cja@buaa.edu.cn
www.sciencedirect.com

Influence of residual stresses on failure pressure of cylindrical pressure vessels

M. Jeyakumar [a,*], T. Christopher [b]

[a] Department of Mechanical Engineering, Sardar Raja College of Engineering, Alangulam, Tirunelveli 627 808, India
[b] Department of Mechanical Engineering, Government College of Engineering, Tirunelveli 627 007, India

Received 26 October 2012; revised 21 January 2013; accepted 13 March 2013
Available online 30 October 2013

KEYWORDS

Aerospace engineering;
ASTM A36;
Finite element analysis;
Pressure vessels;
Welding residual stress

Abstract The utilization of pressure vessels in aerospace applications is manifold. In this work, finite element analysis (FEA) has been carried out using ANSYS software package with 2D axisymmetric model to access the failure pressure of cylindrical pressure vessel made of ASTM A36 carbon steel having weld-induced residual stresses. To find out the effect of residual stresses on failure pressure, first an elasto-plastic analysis is performed to find out the failure pressure of pressure vessel not having residual stresses. Then a thermo-mechanical finite element analysis is performed to assess the residual stresses developed in the pressure vessel during welding. Finally one more elasto-plastic analysis is performed to assess the effect of residual stresses on failure pressure of the pressure vessel having residual stresses. This analysis indicates reduction in the failure pressure due to unfavorable residual stresses.

1. Introduction

Cylindrical pressure vessels are used in various fields such as chemical and nuclear industries, rocket motor case manufacturing and production of many weapon systems. Evaluation of failure pressure that a cylindrical pressure vessel can withstand is an important consideration in the design of pressure vessels. While prediction of failure pressure of pressure vessels, it is also necessary to consider the residual stresses already present in the pressure vessels. Various methods are being used to estimate the failure pressure.[1–4] Finite element techniques based on GPD (Global Plastic Deformation) are also used to evaluate failure pressure and its results were found to be in good agreement with test results.[5] Welding has been widely employed in fabricating ships, off shore structures, steel bridges and pressure vessels. Residual stresses usually of yield strength in magnitude can arise in the weld due to localized heating by welding process and subsequent rapid cooling. The finite element method (FEM) has been used for analyzing various types of welded joints.[6–9] Jiang et al.[10] and Iranmanesh and Darvazi[11] have performed the finite element simulation of temperature field and residual stresses of butt-welded plates. Deng and Murakawa[12] have utilized ABAQUS to generate 2D axisymmetric finite element (FE) models to simulate temperature fields and residual stress states in multi-pass welds in SUS304 stainless steel pipe. They have also performed experiments and demonstrated the adequacy of their analysis results.

* Corresponding author. Tel.: +91 9443612959.
E-mail address: jksrce1964@gmail.com (M. Jeyakumar).

Peer review under responsibility of Editorial Committee of CJA.

ELSEVIER Production and hosting by Elsevier

1000-9361 © 2013 Production and hosting by Elsevier Ltd. on behalf of CSAA & BUAA. Open access under CC BY-NC-ND license.
http://dx.doi.org/10.1016/j.cja.2013.07.025

Table 1 Details of cylindrical pressure vessels, materials and strength properties.[25]

Cylinder No.	Cylindrical shell dimensions (mm)		Material	Tensile strength properties (MPa)	
	Outer diameter	Thickness		Yield strength	Ultimate strength
1	68.00	21.00	Cr–Ni–Mo–V steel	329.6	641.9
2	68.00	21.00	Cr–Ni–Mo–V steel	1101.8	1223.8
3	101.60	31.68	SAE 3320	548.1	726.7
4	31.75	9.50	SAE 4340	716.4	855.6
5	31.75	9.50	SAE 4340	596.4	795.0
6	31.75	9.50	SAE 4340	797.0	859.0
7	101.60	31.68	SAE 1045	419.9	701.9
8	101.60	31.68	SAE 1045	562.6	842.5

They also indicated the possibility of saving a large amount of computational time with reasonable accuracy using the 2D models. Jeyakumar et al.[13] have performed a 2D finite element analysis and predicted weld-induced residual stresses in butt welded two similar 2.25 Cr1Mo low-alloy ferritic steel plates and also ASTM A36 steel plates. Jiang and Yahiaoui[14] have generated a full 3D thermo-mechanical FE model to predict through thickness welding residual stress distributions in a thick-walled tee branch junction employing the element removal/reactivative technique for simulating the deposition of filler material. Melicher et al.[15] have utilized ANSYS to generate 3D FE models for coupled thermo-mechanical analysis of circumferential weld joints. Yaghi et al.[16] have evaluated residual stresses in an axisymmetric single-U multi-pass butt weld of a P91 steel pipe, considering the temperature dependent material properties and allowing solid state phase transformation (SSPT), in addition to the inclusion of heat treatment holding time for studying the effects of post-weld heat treatment (PWHT).

Lu and Hassan[17] have performed thermal and residual stress analyses for butt-welded and socket-welded pipes, and validated their analysis results with existing test results. Nadimi et al.[18] have performed a FEA of residual stresses in butt welding of two dissimilar steel pipes employing element birth and death technique for simulation of filler metal deposition. Fanous et al.[19] have carried out 3D FE modeling and simulation of the welding process with and without metal deposition. Element movement technique is used for metal deposition to minimize the computational time. Tahami and Sorkhabi[20] have carried out 3D FEA to study the effect of the plate thickness on the residual stress in butt-welded steel plates. Moraitis and Labeas[21] developed a two-level three-dimensional Finite Element (FE) model to predict keyhole formation and thermo-mechanical response during Laser Beam Welding (LBW) of steel and aluminium pressure vessel. Wang et al.[22] adopted the FEM to analyze the static strength and stability of the vacuum plume effects experimental system vacuum chamber. Katsuyama et al.[23] evaluated effects of the weld residual stress and scatter of primary water stress corrosion cracking (PWSCC) growth rate on the crack penetration through some case studies. Welding simulation is still CPU time demanding and complex. Simplified 2D welding simulation procedures are required in order to reduce the complexity and maintain the accuracy of the residual stress predictions.[24]

Obviously, there may be many problems in the application of new concepts to the production of pressure vessels and many of them did not consider the residual stress developed in the pressure vessels. Reducing these stresses could result in significant increases in structural strength. In this paper, FEA has been carried out using ANSYS software package with 2D axisymmetric model to access the weld induced residual stresses in butt welding of cylindrical pressure vessels made of ASTM A36 carbon steel and prediction of failure pressure with and without weld-induced residual stresses. Also failure pressure of pressure vessels in Table 1 were evaluated through FEA and its results are compared with available analytical and experimental results and found they are in good agreement.[25]

2. FEA procedure for failure pressure estimates of a cylindrical pressure vessel

Fig. 1 gives the geometrical model and Fig. 2 gives the FEA model of the ASTM A36 carbon steel pressure vessel considered for analysis. FE axisymmetric model is created with 2D element PLANE82 which is an 8 node structural solid having two degrees of freedom at each node, translation in the nodal x and y directions. The FEA model contains 1742 nodes and 520 elements. Axial displacement is suppressed at both ends of the cylindrical shell to arrest the axial growth under internal pressure. The closed end effects are not taken into account in this analysis, since the axial strain was small and could be neglected in closed end cylindrical vessels.[4]

$$\sigma = E\varepsilon\left[1 + \left(\frac{\varepsilon}{\varepsilon_0}\right)^n\right] \tag{1}$$

where $\varepsilon_0 = \sigma_u/E$, σ_u is the ultimate strength of the material and n is the parameter defining the shape of the non-linear stress–strain relationship. $\varepsilon_0 = 0.002143$, $n = 1.798$, $\sigma_u = 450$ MPa and $\sigma_y = 380$ MPa for ASTM A36 carbon steel. Eq. (1) expresses Inverse Romberg–Osgood relationship.[3] It is a

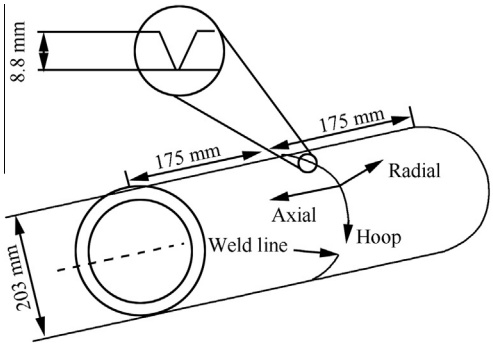

Fig. 1 Geometrical model of ASTM A36 carbon steel pressure vessel.

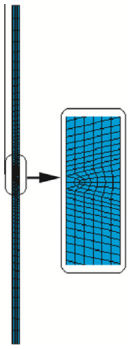

Fig. 2 Axisymmetric FE model of ASTM A36 carbon steel pressure vessel.

constitutive relationship which gives the stress as an explicit function of strain.

The stress–strain curve (see Fig. 3) generated using Eq. (1) is given as input in FEA to consider material behavior during the application of internal pressure. The internal pressure is applied to the FE model using the following steps in ANSYS:Preprocessor → Loads → Define Loads → Apply → Structural → Pressure → On Lines. ANSYS has the provision for checking the global plastic deformation (GPD). It indicates the pressure level to cause complete plastic flow through the cylinder walls (i.e., bursting pressure). Bursting pressure of unflawed pressure vessel without residual stress can be expressed as literature[25]

$$p_b = \frac{2\sigma_y}{\sqrt{3}} \ln R\left(2 - \frac{\sigma_y}{\sigma_u}\right) \tag{2}$$

where σ_u is the ultimate strength of the material, σ_y is the yield strength of the material, and R is wall ratio of hollow cylinder (R_0/R_i).

The effective stress for the cylindrical pressure vessel is expressed as

$$\sigma_1^2 + \sigma_2^2 + \sigma_3^2 - \sigma_1\sigma_2 - \sigma_2\sigma_3 - \sigma_3\sigma_1 = \sigma_y^2 \tag{3}$$

where σ_1 is the hoop stress, σ_2 is the meridional stress and σ_3 is the radial stress. The pressure vessel before welding (i.e., without residual stress) is considered for analysis (Fig. 1) and its failure pressure is obtained first by elasto-plastic analysis. Then a thermo-mechanical FEA is carried out to assess the weld-induced residual stress and another elasto-plastic analysis is performed to assess the effect of residual stress in failure pressure for this pressure vessel having residual stress.

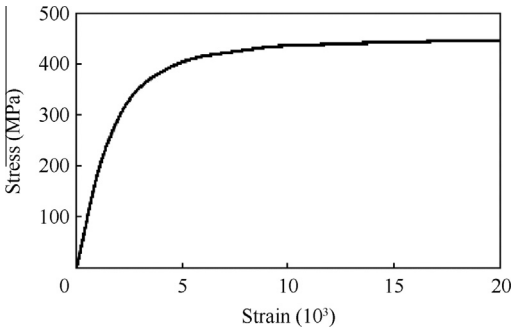

Fig. 3 Stress–strain curve of ASTM A36 carbon steel generated by Eq. (1).

3. Thermo-mechanical analysis

The most important parameter to determine the temperature distribution in the welded components is the heat input. This heat quantity is the output from a particular heat source used to fabricate welded joints. In all the welding processes, heat source provides the required energy and causes localized high temperature spot. In arc-welding with constant voltage (V) and amperage (I), the efficiency of the heat source would be

$$\eta = \frac{Q_s t_{weld}}{VIt_{weld}} = \frac{Q_s}{VI} \tag{4}$$

where Q_s is the heat generating rate and t_{weld} is the welding time and η is the thermal efficiency. The Gaussian heat source is used to simulate the welding-arc, where the heat source density, $q(x,y)$ at an arbitrary point (x,y) is represented by literature[26]

$$q(x,y) = \frac{3Q_s}{\pi r_b^2} \exp\left(-3\frac{r^2}{r_b^2}\right) \tag{5}$$

The distribution of $q(x,y)$ in Eq. (5) represents 95% of the total heat Q_s when applied within a circle with radius r_b. r is the radial distance from the centre of the heat source. It is expressed as $r = \sqrt{x - x_h + y^2}$; x_h is the incremental distance of heat source, which is given by $x_h = v(t - t_0)$; and v is the welding speed.

The surface heat flux, $q_n\left(\equiv -k\nabla T \cdot \bar{n} = -k\frac{\partial T}{\partial n}\right)$ depends on the temperature of the body and the surrounding, which is written in a format more convenient for finite element implementation as

$$q_n = h_c(T - T_{ref}) + e_f s_b\left(T^4 - T_{ref}^4\right) = h_{eff}(T - T_{ref}) \tag{6}$$

The first term in the right hand side of Eq. (6) is convective heat loss, whereas the second term is the heat loss due to radiation. h_c is the heat transfer coefficient, s_b is Stefan-Bolzmann's constant and e_f the emissivity factor. The effective heat transfer coefficient, $h_{ref} = h_c + e_f S_b\left(T^3 + T^2 T_{ref} + TT_{ref}^2 + T_{ref}^3\right)$, is a combination of both the convection and radiation coefficients.

The calculation of welding residual stresses is usually based on the temperature distribution and the thermal stress increment $\Delta\sigma(= E\alpha\Delta T)$. The thermal stress increment is calculated from the incremental thermal strain $(\alpha\Delta T)$, coefficient of thermal expansion α and the Young's modulus (E).

The calculation of residual stress starts with time $t = 0$ and the thermal stress is calculated for the initial temperature distribution of the welded components. At the next time step, the thermal stress increment is added to the initial stress at step $t = 0$. The magnitude of the cumulative thermal stress is limited to the yield strength of the material at actual temperatures. At each step, the forces caused by the induced thermal stresses must be in equilibrium. This procedure is repeated until the last step at which the thermal stress is that at ambient temperature (i.e., the residual stress). Residual stress evaluation involves superposition of the incremental thermal stresses to previous thermal stresses and equilibrium stresses.

4. Finite element solution

This paper deals with the manual metal arc welding (MMAW) simulation of butt-weld joint of ASTM A36 carbon steel cylindrical shells as shown in Fig. 1. Tables 2 and 3 give the chemical composition (wt.%) and temperature dependent properties of the ASTM A36 carbon steel. For thermal analysis, 2D element of Plane 77 is used. It is an 8 node thermal solid (8 node quadrilateral element) with single degree of freedom having temperature at each node. Generally, temperature around the arc is higher than the melting temperature of materials and drops sharply in regions away from weld pool. In high temperature gradient regions of fusion zone (FZ) and heat affected zone (HAZ), more refined mesh close to weld line is essential for obtaining accurate temperature field. For structural analysis, 2D element of Plane 82 is used. It is an 8 node structural solid (8 node quadrilateral element) with two degrees of freedom at each node, translation in the nodal x and y directions.

The arc-power, Q_s (Watts) is evaluated from Eq. (4) by specifying the arc efficiency, $\eta = 0.85$: the arc voltage, $V = 24$ V and the current, $I = 180$ A. The radial heat flux distribution in Eq. (5) is considered on the top surface of the weld. The heat density drops to 5% of its maximum value at $r = r_b$. In the present analysis, r_b is set to 3 mm and welding speed, $v = 5$ mm/s. When the value of r is less than or equal to r_b, the heat flux is calculated according to the Eq. (5). Otherwise, the heat load is set to zero. Filler weld material is assumed to have the same chemical composition of the parent material. The melting temperature of the material is 1783 K. A cut-off temperature ($T_{cut\text{-}off}$) is set to 1073 K. For convective and radiative heat losses, the constants in the complex boundary conditions for the outward flux in Eq. (6) are: Stefan–Boltzman constant, $s_b = 5.67 \times 10^{-8} W/m^2K^4$; convection coefficient, $h_c = 15\ W/m^2K$; and the emissivity factor, $e_f = 0.2$.

By taking the advantage of weak structural to thermal field coupling the complex coupled thermo-mechanical analysis of welding is broken into two parts. In the first part non-linear transient thermal analysis is performed to predict the temperature history of the domain for complete thermal cycle of the welding process. To obtain thermal history, transient, non–linear thermal problem is solved using temperature dependent thermal properties and considering heat conduction, convective and radiative boundary conditions. In thermal analysis the heat flux is specified in 2157 time steps. It takes 6009 s to cool down from the maximum temperature to ambient (room) temperature. In the second part, non-linear structural analysis is performed in which temperature history calculated during thermal analysis is applied as body load along with temperature dependent mechanical properties to obtain the transient and residual stress fields. Load step in structural analysis is kept the same as that of respective thermal load step. Since load steps are too many, ANSYS Parametric Design Language (APDL) has been adopted to perform both thermal and structural analyses. For failure pressure analysis for this pressure vessel along with the residual stress present to assess the effect of residual stress on failure pressure, the analysis is restarted from the terminating (final) load step of thermal stress analysis along with applied internal pressure and performed up to GPD. The pressure corresponding to GPD will be the failure pressure.

Table 2 Chemical composition of ASTM A36 carbon steel.[18]

Element	C	Mn	P	S	Si
wt.%	0.28	0.60–0.90	0.04	0.05	0.40

5. Results and discussion

Fig. 4 shows temperature variation from the weld center line to the ends of the ASTM A36 carbon steel pressure vessel. The results indicate that the pressure vessel is undergoing significant temperature variation. At the beginning, the temperature reduction in the area close to the weld axis shows the quenching

Table 3 Temperature dependent properties of ASTM A36 carbon steel.[18]

Temp (K)	Specific heat (J/(kg·K))	Thermal conductivity W/(mK)	Density (kg/m^3)	Heat transfer coefficient W/(m^{2}K)	Elastic modulus (GPa)	Poisson's ratio	Thermal expansion coefficient ($10^{-6}K^{-1}$)	Yield stress (MPa)
273	480	60	7880	15.9	210	0.280	1.10	380
373	500	50	7880	16.5	200	0.285	1.15	340
473	520	45	7800	17.3	200	0.290	1.20	315
673	650	38	7760	20.1	170	0.310	1.30	230
873	750	30	7600	24.6	80	0.330	1.42	110
1073	1000	25	7520	31.4	35	0.330	1.45	30
1473	1400	28	7300	53.6	15	0.360	1.45	20
1573	1600	37	7250	61.2	10	0.380	1.45	18
1823	1700	37	7180	84.8	10	0.390	1.45	15

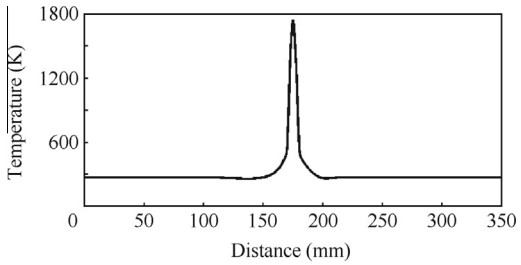

Fig. 4 Variation of temperature distribution from weld center line to the ends of the ASTM A36 carbon steel pressure vessel.

effect. Fig. 5 shows the residual hoop stress from the weld center line to the ends of the ASTM A36 carbon steel pressure vessel.

The present analysis results indicate the hoop residual stress varies from 432 MPa (tensile) to −79 MPa (compressive) at inner wall and from 285.5 MPa (tensile) to −156 MPa (compressive) at outer wall. Fig. 6 shows the residual meridional stress from the weld center line to the ends of the ASTM A36 carbon steel pressure vessel. The present analysis results indicate the meridional residual stress varies from 340 MPa (tensile) to −104 MPa (compressive) at inner wall and from 46 MPa (tensile) to −323 MPa (compressive) at outer wall. Fig. 5 and Fig. 6 also show that the tensile stresses were developed in the weld zone. These tensile residual stresses are playing the major role in the reduction of failure pressure. These tensile stresses gradually decrease away from the weld center line and become compressive towards the edge of the plate. Fig. 7 shows the residual effective stress from the weld center

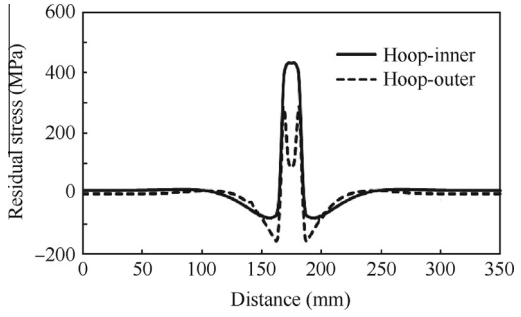

Fig. 5 Welding residual hoop stress at walls of ASTM A36 carbon steel pressure vessel.

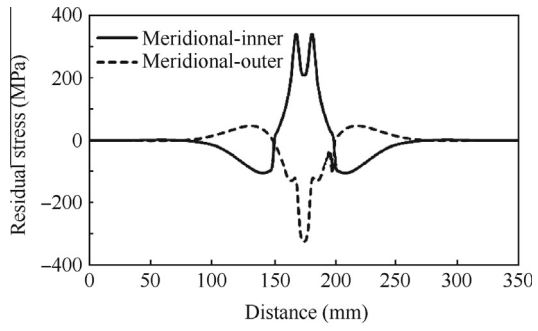

Fig. 6 Welding residual meridional stress at walls of ASTM A36 carbon steel pressure vessel.

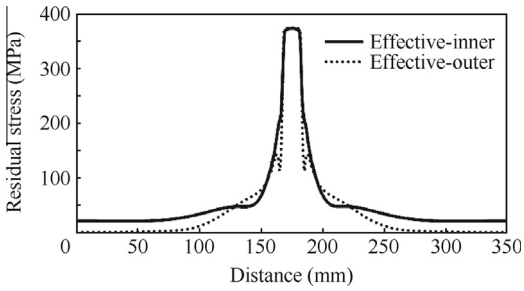

Fig. 7 Welding residual effective stress at walls of ASTM A36 carbon steel pressure vessel.

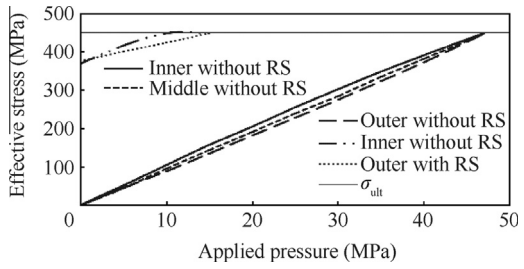

Fig. 8 Effective stress plot of ASTM A36 carbon steel pressure vessel with and without residual stress up to global plastic deformation.

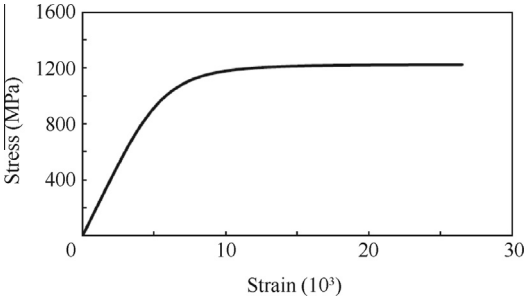

Fig. 9 Stress–strain curve of Cr–Ni–Mo–V steel generated by Eq. (1).

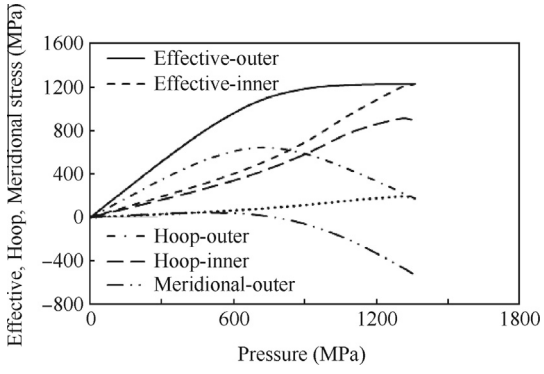

Fig. 10 Effective, hoop and meridional stress plot of Cr–Ni–Mo–V steel pressure vessel[25] (No. 2) with the applied internal pressure up to global plastic deformation.

Table 4 Material constants in Eq. (1) for the stress–strain curve and failure pressure of cylindrical vessels in Tables 2 and 3.

Cylinder No.	Material constants in Eq. (1)			Failure pressure (MPa)		
	E (GPa)	ε_0	n	Observed[25]	Calculated[25]	FEA
1	207	0.00310	0.945	689.5	561.9	711.0
2	207	0.00592	3.600	1379.0	1325.2	1358.0
3	207	0.00351	1.710	730.8	770.8	820.0
4	207	0.00414	2.340	917.0	954.9	901.0
5	207	0.00384	1.754	827.4	856.3	836.0
6	207	0.00415	3.512	806.7	892.2	904.0
7	207	0.00339	1.164	737.7	662.6	791.0
8	207	0.00407	1.464	820.5	846.0	950.0

line to the ends of the ASTM A36 carbon steel pressure vessel. The present analysis results indicate the residual effective stress varies from 374 MPa (tensile) to 21 MPa (tensile) at inner wall and from 374 MPa (tensile) to zero at outer wall. Fig. 8 shows the effective stress at failure with and without residual stress of the ASTM A36 carbon steel pressure vessel. The present analysis results indicate the failure pressure as 48 MPa without residual stress while it is 46 MPa by using Eq. (2), having good agreement, and the failure pressure with residual stress reduces to 15 MPa. This shows the influence of residual stress in reduction of failure pressure. Table 4 gives material constants in Eq. (1) for the stress–strain curve and failure pressure of cylindrical vessels in Table 1.[25] Fig. 9 gives the stress–strain curve of Cr–Ni–Mo–V steel generated by Eq. (1). Fig. 10 gives effective, hoop and meridional stress plot of Cr–Ni–Mo–V steel pressure vessel (No. 2) in Tables 1 and 4 with the applied internal pressure up to global plastic deformation. The failure pressure evaluated through the present analysis (FEA) is 1358 MPa, where the experimental and calculated[25] values are 1379 and 1325.2 MPa, respectively and they are found in good agreement.

Eight number of pressure vessels were analyzed in literature[25] as shown in Tables 1 and 4 for the influence of residual stress on the behavior of cylinders, in which three cylinders of each material were heat treated under identical conditions. One cylinder was then used for the residual stress test, the second for the static internal pressure test and the third one was used to determine the mechanical properties resulting from the heat treatment. It is concluded that the residual stresses in pressure vessels due to heat treatment do not appear to influence overstrain or bursting pressure. It should be noted that the material properties used in literature[25] were measured after the heat treatment process. Now while calculating the failure pressure analytically, in which if these material properties were used then the effect of residual stresses on failure pressure will not be felt, since the residual stress influence will be there in material property itself. If the properties of this material before heat treatment would have been used, then the effect would be felt.

6. Concluding remarks

2D Finite element analysis with axisymmetric model has been carried out using ANSYS software package to access the failure pressure of cylindrical pressure vessel made of ASTM A36 carbon steel having weld-induced residual stresses. An elasto-plastic analysis is performed to find out the failure pressure of the pressure vessel without residual stresses.

The results obtained from FEA agree well with the results obtained from Eq. (2). To assess the residual stresses present in the pressure vessel due to welding, a thermo-mechanical finite element analysis is performed. Another elasto plastic analysis is also performed to assess the effect of residual stresses on failure pressure of the pressure vessel with residual stresses. From this analysis, it is observed that there is a reduction in failure pressure due to unfavorable residual stresses. Also failure pressure of pressure vessels (No. 2) in Table 1 was evaluated through FEA and its results are compared with analytical and experimental results and they are found in good agreement. The results presented can be synthesized to provide some approximate guidelines for the use of aerospace pressure vessel applications.

References

1. Faupel JH. Yield and bursting characteristics of heavy walled cylinders. *J Appl Mech-T ASME* 1956;**78**(5):1031–64.
2. Svensson NL. The bursting pressure of cylindrical and spherical vessels. *J Appl Mech-T ASME* 1958;**25**(1):89–96.
3. Beena AP, Sundaresan MK, Rao B. Destructive tests of 15CDV6 steel rocket motor cases and their application in light weight design. *Int J Press Vessels Pip* 1995;**62**(3):313–20.
4. Christopher T, Rama Sarma BSV, Govindan Potti PK, Nageswara Rao B, Sankaranarayanasamy K. A comparative study on failure pressure estimation of unflawed cylindrical vessels. *Int J Press Vessels Pip* 2002;**79**(1):53–66.
5. Brabin AT, Christopher T, Nageswara Rao B. Investigation on failure behavior of unflawed steel cylindrical pressure vessel using FEA. *Multidiscip Model Mater Struct* 2009;**5**(1):29–42.
6. Lindgren LE. Finite element modeling and simulation of welding, Part 2: Improved material modeling. *J Therm Stresses* 2001;**24**(3):195–231.
7. Radaj D. *Welding residual stresses and distortion*. Berlin: Springer-Verlag; 2003.
8. Duranton P, Devaux J, Robin V, Gilles P, Bergheau JM. 3D modeling of multipass welding of a 316L stainless steel pipe. *J Mater Process Tech* 2004;**153–154**:457–63.
9. Murugan N, Narayanan R. Finite element simulation of residual stresses and their measurement by contour method. *Mater Design* 2009;**30**(6):2067–71.
10. Jiang W, Yahiaoui K, Hall FR. Finite element predictions of temperature distributions in a multipass welded piping branch junction. *J Pressure Vessel Technol* 2005;**127**(1):7–12.
11. Iranmanesh M, Darvazi AR. Analytical and numerical simulation of temperature field and residual stresses of butt weld in steel

plates used in ship manufacturing. *Asian J Appl Sci* 2008;**1**(1):70–8.
12. Deng D, Murakawa H. Numerical simulation of temperature field and residual stress in multi-pass welds in stainless steel pipe and comparison with experimental results. *Comp Mater Sci* 2006;**37**(3):269–77.
13. Jeyakumar M, Christopher T, Narayanan R, Nageswara Rao B. Residual stress evaluation in butt-welded steel plates. *Indian J Eng Mater Sci* 2011;**18**:425–34.
14. Jiang W, Yahiaoui K. Finite element prediction of residual stress distribution in a multi-pass welded piping branch junction. *J Pressure Vessel Technol* 2007;**129**:601–8.
15. Melicher R, Mesko J, Novak P, Zmindak M. Residual stress simulation of circumferential welded joints. *Appl Comput Mech* 2007;**1**:541–8.
16. Yaghi AH, Hyde TH, Becker AA, Sun W. Finite element simulation of welding residual stresses in a P91 steel pipe incorporating solid-state phase transformation and post-weld treatment. *J Strain Analysis* 2008;**43**(5):275–93.
17. Lu X, Hassan T. Residual stresses in butt and socket welded joints. In: *16th international conference on structural mechanics in reactor technology*; 2001. p. 1−8.
18. Nadimi S, Khoushehmehr RJ, Rohani B, Mostafapour A. Investigation and analysis of weld induced residual stresses in two dissimilar pipes by finite element modeling. *J Appl Sci* 2008;**8**(6):1014–20.
19. Fanous IFZ, Younan MYA, Wifi AS. 3D finite element modeling of the welding process using element birth and element movement techniques. *J Pressure Vessel Technol* 2003;**125**:144–50.
20. Tahami FV, Sorkhabi AHD. Finite element analysis of thickness effect on the residual stress in butt-welded 2.25Cr1Mo steel plates. *J Appl Sci* 2009;**9**:1331–7.
21. Moraitis GA, Labeas GN. Prediction of residual stresses and distortions due to laser beam welding of butt joints in pressure vessels. *Int J Press Vessels Pip* 2009;**86**(2):133–42.
22. Wang W, Cai GB, Zhou JP. Large-scale vacuum vessel design and finite element analysis. *Chin J Aeronaut* 2012;**25**(2):189–97.
23. Katsuyama J, Udagawa M, Nishikawa H, Nakamura M, Onizawa K. Evaluation of weld residual stress near cladding and J-weld in reactor pressure vessel head for the assessment of PWSCC behavior. *E-J Adv Maintenance* 2010;**2**(2):50–64.
24. Lindgren LE. Finite element modeling and simulation of welding, Part 1: increased complexity. *J Therm Stresses* 2001;**24**(2):141–92.
25. Faupel JH. Influence of residual stress on behavior of thick-wall closed-end cylinders. *J Appl Mech-T ASME* 1953;**75**:345–54.
26. Nguyen NT. *Thermal analysis of welds*. Southampton: WIT Press; 2004.

Jeyakumar M. has received his B.E. degree in Mechanical Engineering from M.S. University, Tirunelveli, India and holds a M.S. degree in production Engineering from M.K.University, Madurai, India. He has received Ph.D. degree from Anna University, Chennai, India. He is a Professor in Mechanical Engineering Department and Principal of Sardar Raja College of Engineering, Alangulam, Tamilnadu, India. His current research areas include finite element analysis, material science and welding.

Christopher T. is working as professor and head of Mechanical department in Government College of Engineering, Tirunelveli, Tamilnadu, India. He has been a committee member for various international and national conferences. He has 30 research publications in international/national journals and conferences. His areas of interest include finite element analysis, welding and material science.